Fortunati, E.; Gigli, M.; Luzi, F.; Dominici, F.; Lotti, N.; Gazzano, M.; Cano Embuena, AI.... (2017). Processing and characterization of nanocomposite based on poly(butylene/triethylene succinate) copolymers and cellulose nanocrystals. Carbohydrate Polymers. 165:51-60. https://doi.org/10.1016/j.carbpol.2017.02.024

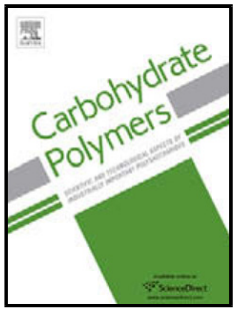

Title: Processing and characterization of nanocomposite based on poly(butylene/triethylene succinate) copolymers and cellulose nanocrystals

Authors: Elena Fortunati, Matteo Gigli, Francesca Luzi, Franco Dominici, Nadia Lotti, Massimo Gazzano, Amalia Cano, Amparo Chiralt, Andrea Munari, Josè Maria Kenny, Ilaria Armentano, Luigi Torre

PII: S0144-8617(17)30144-3
DOI: http://dx.doi.org/doi:10.1016/j.carbpol.2017.02.024
Reference: CARP 12003

To appear in:

Received date: 1-9-2016
Revised date: 6-2-2017
Accepted date: 6-2-2017

Please cite this article as: Fortunati, Elena., Gigli, Matteo., Luzi, Francesca., Dominici, Franco., Lotti, Nadia., Gazzano, Massimo., Cano, Amalia., Chiralt, Amparo., Munari, Andrea., Kenny, Josè Maria., Armentano, Ilaria., & Torre, Luigi., Processing and characterization of nanocomposite based on poly(butylene/triethylene succinate) copolymers and cellulose nanocrystals.*Carbohydrate Polymers* http://dx.doi.org/10.1016/j.carbpol.2017.02.024

Processing and characterization of nanocomposite based on poly(butylene/triethylene succinate) copolymers and cellulose nanocrystals

Elena Fortunati[a], Matteo Gigli[b*], Francesca Luzi[a], Franco Dominici[a], Nadia Lotti[c], Massimo Gazzano[d], Amalia Cano[e], Amparo Chiralt[e], Andrea Munari[c], Josè Maria Kenny[a], Ilaria Armentano[f*], Luigi Torre[a]

[a]*University of Perugia, Civil and Environmental Engineering Department, UdR INSTM, University of Perugia, Strada di Pentima 4, 05100 Terni, Italy.*

[b]*Department of Chemical Science and Technology, University of Rome "Tor Vergata", Via della Ricerca Scientifica 1, 00133 Roma, Italy* (current address, work done at address c)

[c]*Civil, Chemical, Environmental and Materials Engineering Dept. (DICAM), University of Bologna, Via Terracini 28, 40131 Bologna, Italy.*

[d]*Organic Synthesis and Photoreactivity Institute, CNR, Via Selmi 2, 40126, Bologna, Italy.*

[e]*Institute of Food Engineering for Development, Universitat Politècnica de València, Camino de Vera, s/n. 46022 Valencia, Spain.*

[f]*Department of Ecological and Biological Sciences (DEB), Tuscia University, Viale dell'Università, snc, 01100 Viterbo, Italy*

**Corresponding Authors: Ilaria Armentano, ilaria.armentano@unitus.it*

Matteo Gigli, matteo.gigli@uniroma2.it

Highlights

1. Random eco-friendly copolyesters were successfully synthesized
2. Nanocomposites based on cellulose nanocrystals (CNC) were developed by extrusion
3. CNC modulated polymer mechanical properties
4. Extruded films displayed a tunable range of degradation rate

Abstract

A new class of biodegradable materials developed by a combination of random eco-friendly copolyesters containing butylene succinate (BS) and triethylene succinate (TES) sequences with cellulose nanocrystals (CNC), is proposed and studied. Polymers and nanocomposite films were prepared by an optimized extrusion process to improve the processability and mechanical response for flexible film manufacturing. Poly(butylene succinate) (PBS) homopolymer and two random copolyesters containing different amounts of TES co-units, P(BS85TES15) and P(BS70TES30), were synthesized by melt polycondensation. The effect of TES and CNC presence and content on the microstructure, tensile properties, thermal characteristics and disintegration under composting conditions, as well as on the toughening mechanism of the blends was investigated.

Material properties were modulated by varying the chemical composition. CNC were used as reinforcement additive and their effect is modulated by the interaction with the three polymeric matrices. The extruded films displayed tunable degradation rates, mechanical properties and wettability, and showed promising results for different industrial applications.

Keywords: random copolyesters; cellulose nanocrystals; bionanocomposite; extrusion process.

1.Introduction

The development of new bio-based, biodegradable and sustainable polymeric systems, by using innovative processing technologies, is an important strategy to reduce the dependence of fossil fuels and support the transition towards a greener and more sustainable future.

In this respect, poly(butylene succinate) (PBS) is undoubtedly an interesting member of the aliphatic polyester class. In view of its good mechanical properties that are comparable with low-density polyethylene and other polyolefins, good thermal resistance and melt processability (Zhang&Zhang, 2016; Gigli, et al., 2016), PBS can be considered a promising candidate for the packaging industry. To widen the PBS application range and to improve some of its properties, such as the slow biodegradation rate, different pathways have been followed. Copolymerization and realization of blends and composites are the most explored strategies in this respect (Gigli, et al., 2016; Fabbri, et al., 2014; Khalil, et al., 2014; Kim, et al., 2006; Zakharova, et al., 2015). In particular, the introduction of ether and thio-ether linkages has proven to be a winning strategy to upgrade the characteristics of PBS and of other aliphatic polyesters. By mainly acting on the degree of crystallinity and on the surface wettability, it has been possible to deeply modify the mechanical properties and the biodegradability of the parent homopolymer. (Gigli, et al., 2014; Gigli, et al., 2013).

Cellulose is the most abundant and inexhaustible carbohydrate polymer in nature. Its physical and chemical properties permit to develop different kind of materials and products (Klemm et al. 2005). In particular, cellulose nanocrystals (CNC) are widely employed as reinforcing agents in lightweight and bio-based polymeric nanocomposites (Habibi, Lucia, & Rojas 2010; Moon, et al., 2011). CNC show nanosized dimensions with rod-like shape, high aspect ratio, low density (1.566 g/cm^3), and reactive surface (Bitinis, et al., 2013), and mechanical properties comparable to other reinforcement materials.

The dispersion in the thermoplastic polymers is a key issue to be improved and evaluated in order to transfer the CNC properties to the polymeric materials and to obtain multifunctional nanostructured polymers with modulated behavior (Dufresne, 2013). In particular, the dispersion of the CNC in hydrophobic thermoplastic polymers is difficult due to the dominant hydrophilic nature of cellulose (Song, Xiao, & Zhao, 2014), and this can limit their efficiency as reinforcing elements (Dufresne, 2013). Different CNC surface modification methods, by using both chemical and physical approaches, have been developed including esterification, etherification, silylation, polymer grafting, adsorbing surfactants or polymer coating (Braun, Dorgan, & Hollingsworth, 2012; Fortunati, et al., 2012; Lizundia, et al., 2016).

The goal of this research is to develop high innovative renewable bionanocomposites by combining newly synthesized biodegradable copolymers with cellulose nanocrystals as reinforcement phase. The thermal, mechanical, chemical and disintegration properties of the novel developed films were investigated and correlated to CNC content and polymer chain microstructure. The final results could take to the production of biodegradable nanocomposites with cellulose nanocrystals as reinforcing fillers that display comparable properties to inorganic-based reinforced nanocomposites.

2. Experimental section

2.1. Materials and methods

2.1.1. Polymer synthesis

Dimethylsuccinate (DMS), 1,4-butanediol (BD), triethylene glycol (TEG), glycerol and titanium tetrabutoxide (TBT) (Sigma-Aldrich) were reagent grade products. All the reagents were used as supplied with the exception of TBT that was distilled before use.

Poly(butylene succinate) (PBS) and poly(butylene/triethylene glycol succinate) random copolymers (P(BSxTESy)) were synthesized in bulk by two step melt polycondensation, by employing DMS and BD (PBS synthesis) or DMS and different ratios of BD and TEG (P(BSxTESy) synthesis). In particular, two copolymers containing respectively 15% and 30% of TES co-units have been prepared.A 20 mol% excess of total glycol with respect to DMS was used. A low amount of glycerol (1 mg/g of polymer) was also added to the reaction mixture. TBT was employed as catalyst (about 150 ppm of Ti/g of polymer).

The first stage was run at 180°C under pure nitrogen flow. When more than 90% of the theoretical amount of methanol was distilled off, the pressure was reduced to about 0.08 mbar and the temperature was gradually risen to 230°C to facilitate the removal of the excess of glycol. The reactions were carried out until a constant torque was measured.

2.1.2. Cellulose nanocrystals

Commercial microcrystalline cellulose (MCC, supplied by Sigma–Aldrich®, size 10–15 µm) was used as precursor for cellulose nanocrystal extraction, while an acid phosphate ester of ethoxylated nonylphenol (Beycostat A B09 (CECCA S.A.)) was used for their modification. All the other chemicals used for cellulose nanocrystal synthesis were supplied by Sigma–Aldrich®. Cellulose nanocrystals (CNC), 100 to 200 nm in length and 5–10 nm in width, were obtained by sulfuric acid hydrolysis, and modified by the Beycostat surfactant (s-CNC) (Fortunati, et al., 2014; Heux, et al., 2000). The surfactant was added to the water suspension containing nanocrystals in portion of 1/1 (wt/wt) using an estimated weight of CNC directly after the hydrolysis process.

2.2. Nanocomposite film processing

P(BSxTESy) random copolymers and modified cellulose nanocrystals were dried before processing to eliminate moisture traces and to avoid hydrolysis reactions. Polymers were put into an oven at 50°C for 24 h, while s-CNC was dried at 70 °C for 4 h. P(BSxTESy) copolymers and nanocomposite based formulations were processed and mixed by using a twin-screw microextruder (Dsm Explore 5&15 CC Micro Compounder). Screw speed, mixing time and temperature profile were optimized during the extrusion procedure. Two different s-CNC concentrations were selected: 1%wt, and 5%wt as shown in Table 1. Polymer and nanocomposite films with thicknesses between 20 and 60 μm were obtained by extrusion with the adequate filmature tip. Screw speed at 100 rpm was set to optimize the material properties, while the temperature profile was set up according to the different melting temperature of the selected copolymers, as reported in Table 1, in the three different extrusion areas. The total processing time was equal to 3 min: pure polymers were mixed for 3 min, while for the nanocomposites preparation the s-CNC were added after 1 min.

2.3. Polymer molecular characterization

Polymer structure and composition were determined by means of proton nuclear magnetic resonance (1H-NMR) spectroscopy at 20°C, employing a Varian Inova 400-MHz instrument (Agilent Technologies, USA). Polymer samples were dissolved in deuterated chloroform at a concentration of about 20 mg/mL.

Molecular weights were evaluated by gel-permeation chromatography (GPC) at 30°C using a 1100 HPLC system (Agilent Technologies, USA) equipped with PLgel 5-μm MiniMIX-C column (Agilent Technologies, USA). A refractive index was employed as detector. Chloroform was used as eluent with a 0.3 mL/min flow and sample concentrations of about 2 mg/mL. A molecular weight calibration curve was obtained with polystyrene standards in the range of molecular weight 2000-100,000 g/mol.

2.4. Nanocomposite characterization

All samples were stored over P_2O_5 under vacuum at 20°C before characterization.

2.4.1. Microstructure

Microstructure of the fracture surfaces of polymers and s-CNC based nanocomposite films were investigated by field emission scanning electron microscope (FESEM Supra 25, Zeiss, Germany). Films were previously freeze-cut in liquid nitrogen, gold coated with an Agar automatic sputter coater and then analysed. Optical images were also performed by an inverted microscope, Nikon Epiphot 300.

2.4.2. Thermal characterization

Differential scanning calorimetry (DSC) (DSC6, Perkin Elmer, Waltham, MA, USA) was used for the calorimetric measurements. Aluminium pans containing about 10 mg of polymeric samples were heated up from -70°C to 40°C above fusion temperature (T_m) (I scan), held for 3 min and then rapidly quenched (about 100 °C/min) to -70°C. Finally, the samples were reheated to T_m + 40°C (II scan). Both scans were run at a rate of 20°C/min. The samples were heated to T_m + 40°C and then cooled at 5°C/min after holding for 3 min at a constant temperature in order to determine the crystallization rate under non-isothermal conditions.

Thermal degradation behavior of P(BSxTESy)-based formulations was evaluated by thermogravimetric analysis (TGA, Seiko Exstar 6300, Tokyo, Japan). 5 mg of each sample were used and dynamic tests were performed under nitrogen atmosphere (250 mL min^{-1})

from 30 °C to 600 °C at 10 °C min^{-1}. Thermal degradation temperatures (T_{max}) for each tested material were evaluated.

2.4.3. Wide-angle X-ray diffractometry

X-ray diffraction (XRD) patterns of polymeric films were performed in the wide-angle region by means of a PANalytical X'PertPro diffractometer (Almelo, The Netherlands) equipped with a fast X'Celerator detector. The radiation was supplied by a copper target (λ=0.1548 nm) and 567 points at interval 0.1° (2θ) were scanned for 100s each. The crystallinity index X_c was calculated as the ratio between the area subtended by the peaks and the total diffraction area, cleaned by the incoherent scattering.

2.4.4. FT-IR

Fourier infrared (FT-IR) spectra of the polymer and nanocomposite films in the 400–4000 cm^{-1} range, were recorded using a Jasco FT-IR 615 (Japan) spectrometer with attenuated total reflection spectroscopy (ATR).

2.4.4. Mechanical properties

The tensile properties of polymer and nanocomposite films were evaluated. Tests were performed on 50 x 10 mm^2 rectangular probes as indicated in the UNI EN ISO 527-5 standard, with a crosshead speed of 1 mm min^{-1} and a load cell of 50 N. These tests were carried out in a digital Lloyd testing machine (Lloyd Instrument LR 30K Segensworth West, Foreham, UK) at room temperature, with the initial grip separation of 25 mm. Tensile strength (σ_B), elongation at break (ε_B), and Young's modulus (E) were calculated from the resulting stress-strain curves. At least six samples were analyzed for each formulation.

2.4.5. Optical properties

The internal transmittance and the gloss of polymer and nanocomposite films were investigated. The transparency of the films was determined from the surface reflectance spectra by using a spectrocolorimeter CM-3600d (Minolta Co, Tokyo, Japan) with a 30 mm illuminated sample area by applying the Kubelka–Munk theory for multiple scattering to the reflection spectra. Internal transmittance (T_i) of the films was calculated using Equation 1, where R_0 is the reflectance of the film using an ideal black background. Parameters a and b were quantified by equations 2 and 3, where R is the reflectance of the sample layer backed by a known reflectance R_g. The reflection spectra on the white and black background was determined from 400 to 700 nm. Measurements were taken in triplicate for each film.

$$T_i = \sqrt{(a - R_0)^2 - b^2} \qquad \text{(Eq. 1)}$$

$$a = \frac{1}{2}\left(R + \frac{R_0 - R + R_g}{R_0 R_g}\right) \qquad \text{(Eq. 2)}$$

$$b = (a^2 - 1) \qquad \text{(Eq. 3)}$$

Gloss was measured using a surface gloss meter (Multi-Gloss 268, Minolta, Langenhagen, Germany) at an incidence angle of 60º, according to the ASTM standard D523 (ASTM, 1999). Gloss measurements were performed in triplicate over a black matte standard plate. Results were expressed as gloss units, relative to a highly polished surface of standard black glass with a gloss value close to 100.

2.4.6. Wettability

The wettability of the polymeric and nanocomposite films has been carried out by measuring the water contact angle at room temperature under static conditions. A KSV CAM101 (KSV, Espoo, Finland) instrument coupled with a Drop Shape Analysis software was used for the analysis. The measurements were performed by recording the side profile of

deionized water drops deposited in different areas of the films. The values are reported as the average value of ten independent measurements.

2.4.7. Overall migration

The overall migration analysis of P(BS70TES30), P(BS70TES30)/1s-CNC and P(BS70TES30)/5s-CNC formulations was run in triplicate in simulant A (10% (v/v) ethanol water solution) and alternative simulant to D2 (isooctane) according to current legislation Commission Regulation (EU) N° 10/2011. Rectangular strips of 10 cm^2 in 10 mL of food simulants were used. Samples were kept in the ethanol solution in a controlled atmosphere at 40 °C for 10 days, while samples in isooctane were kept at 20 °C for 2 days according to EN 1186-1:2002. At the end of the experiment, films were removed and the simulants evaporated in agreement with the European Standard 1186-3:2002 (Materials and articles in contact with foodstuffs - Plastics - Part 3: Test methods for overall migration into aqueous food simulants by total immersion). The residues were weighed with an analytical balance and the migration value in mg kg^{-1} of each simulant was determined.

2.3.8. Degradation in compost

The degradation experiments have been carried out on the P(BS70TES30), P(BS70TES30)/1s-CNC and P(BS70TES30)/5s-CNC films at 58.0±0.1°C. The mature compost employed for the tests was supplied by HerAmbiente S.p.A. (Bologna, Italy) and was composed as follows (as declared by HerAmbiente): organic carbon: 22.08% of the dry solid, humic and fulvic carbon: 13.44% of the dry solid, C/N ratio: 12.97, pH: 8.15 and salinity: 2.88 dS/m.

Weighed film specimens of 20 x 30 mm and about 35 mg of weight were used for the experiments.

Each sample was placed in a 100 mL bottle in between two layers of compost. Each layer consisted of 20 g of compost. On top of the second layer, 10 mL of deionized water were added.

The samples were withdrawn from the compost at determined time intervals, washed in accordance to the protocol previously described (Genovese, et al., 2014), and dried over P_2O_5 under vacuum to constant weight. The residual mass was calculated by using the following equation:

$$((m_i - m_f) / m_i)*100 \qquad \text{(Eq. 4)}$$

where m_f is the final weight and m_i is the initial weight. The surface microstructure was analysed by visual observation and by scanning electron microscopy on gold sputtered films glued with carbon tape on aluminum stabs by using a Philips 515 instrument (Amsterdam, The Netherlands).

3. Results and discussion

3.1. Polymer synthesis

The molecular characterization data of the synthesized polyesters are reported in Table 1. The samples were characterized by relatively high molecular weights indicating that appropriate synthesis conditions were achieved. 1H-NMR investigations displayed that the chemical structure is consistent with the expected one and that the composition of the P(BSxTESy) copolymers is close to the feed (Table 1). As an example, the 1H-NMR spectrum of P(BS70TES30) is shown in Figure 1, together with the chemical shift assignments.

The copolymer composition was calculated from the relative areas of the 1H-NMR resonance peak of the **b** aliphatic proton of the butanediol subunit located at 4.11 ppm and of

the **d** protons of the methylene groups of the triethylene glycol subunit at 4.25 ppm, as previously reported (Soccio, et al., 2012). 1H-NMR analysis allowed also for the determination of the arrangement of the comonomeric units along the polymer backbone, by the calculation of the degree of randomness (*b*). The calculation of *b* was carried out taking into consideration the resonance peaks of the aliphatic protons of the succinic subunit in the region δ = 2.61 – 2.65, as reported elsewhere (Soccio, et al., 2012). As expected, due to the catalyst employed and the high temperatures involved in the reactions, the P(BSxTEsy) copolymers showed a random distribution of the comonomeric sequences (Table 1).

3.2. Morphological investigations

Field emission scanning electron microscopy investigations of neat homopolymer, copolymer films and s-CNC based nanocomposites were performed to evaluate the sample morphology and to analyze cellulose nanocrystal dispersion in the polymer matrices.

Microstructural properties are critical since they affect the final material optical, migration and mechanical behavior. Figure 2 shows FESEM images of the cryogenic fractured surfaces of neat polymer and nanocomposite films with 5%wt of cellulose nanocrystals at different magnifications. Neat PBS showed a homogeneous and smooth surface, with the presence of round uniform microstructure of around 500 nm in diameter. The fracture surface of the copolymers P(BS85TES15) and (BS70TES30) changed, displaying a two-phases like microstructure, visible only at higher resolution. FESEM images underline as the copolymer film morphology varies with the TES content, thus affecting all the final film properties. Hence the microstructure variations for the P(BSxTESy) copolymers may be associated to the differences in the viscosity of PBS and P(BSxTESy), along with the varying chemical compositions. After adding a small amount of s-CNC, 1%wt (Figure S1) a different microstructure was observed, without evidence of multiple s-CNC aggregates,

while some individual cellulose nanocrystals can be identified in samples with high content (5%wt, Figure 2). The surfactant used for the CNC dispersion that contains polyethylene glycol units shows good affinity with the co-units due to the very similar chemical structure. Indeed, these last are characterized by the presence of two $-CH_2-CH_2-O-$ sequences per repeating unit that well resemble the PEG chemical structure, thus promoting the interaction between s-CNC and copolymers. This can guarantee an improved CNC dispersion in the copolymer with respect to the PBS homopolymer. Furthermore, individual s-CNC overlap the micro and nanostructure of neat PBS and its copolymers, as identified by some arrows in the fractured surface images.

3.3. Thermal properties, X-Ray characterization and FT-IR analysis

DTG curves obtained by TGA analysis as a function of the temperature for PBS, P(BS85TES15) and P(BS70TES30) polymeric films and their nanocomposites are shown in Figure S2, whereas the maximum degradation temperature values (T_{max}) are summarized in Table 2. Neat PBS homopolymer, P(BS85TES15) and P(BS70TES30) copolymers based films displayed thermal degradation within a relatively narrow interval centered at 402°C, 407°C, and 404°C respectively. This underlines that the presence of TES co-units does not influence the thermal stability of the PBS homopolymer. Moreover, the data observed underline that the addition of s-CNC does not affect the maximum degradation temperatures and the degradation behavior of the different polymer matrices. Table 2 summarizes the thermal properties obtained by DSC analysis.

In order to clarify the nature of the crystalline phase, the structural characterization of P(BSxTESy) copolymers was carried out by wide angle X-ray diffraction. The X-ray diffraction patterns are reported in Figure S3. Both pattern shape and peak position clearly

indicate that the crystalline phase is α-PBS (Ichikawa, et al., 2000) independently of the chemical composition. The presence of the s-CNC does not appreciably alter the pattern, even for the higher s-CNC amount. This effect is probably due to the low content of the s-CNC in the polymers. Furthermore, an overlap of the s-CNC pattern with low intense reflections of α-PBS phase is present (Figure S4).

As to the glass transition, it can be observed that the T_g slightly decreased as TES co-unit content increased. The results are due to an enhanced flexibility given by the triethylene glycol subunit, which is characterized by the presence of two additional ether-oxygen atoms and methylene groups with respect to the butandiol, as already observed in the literature (Gigli, et al., 2014).

Non-isothermal experiments were carried out to evaluate the influence of the TES co-units and of the s-CNC presence on the PBS crystallization ability. To do so, the samples were cooled with a controlled rate from the melt. The exothermic crystallization peaks of the samples under investigation are shown in Figure 3c. The results indicated that the crystallization temperature of PBS is significantly decreased by the presence of TES comonomeric units, while the s-CNC did not have any appreciable influence.

The second scan after quenching from the melt did not highlight any variation with respect to the first scan, indicating that the crystallinity of the samples cannot be suppressed by quenching (Table 2 and Figure 3,b).

FT-IR spectra of the nanocomposite films (Figure S5) show the main peaks of the polymers, confirming the non-covalent interaction with the surfactant modified cellulose nanocrystals.

3.4. Mechanical properties

The mechanical behavior in terms of strength and elongation at break, and Young's modulus of neat polymers and s-CNC based nanocomposites was evaluated. Tensile test results are

reported in Table 2. All studied samples show the typical stress–strain curves of materials with a plastic behavior. PBS homopolymer displayed the highest Young's modulus (430 MPa) and tensile strength (σ_B equal to 40 MPa), as compared to the neat copolymers, but maintained a good value of elongation at break (220%), probably due to the processing technology. In the two investigated copolymers, the Young's modulus regularly decreased, whereas deformation at break regularly increased with the increase of TES content, from 220% to 350% for PBS and P(BS70TES30), respectively. The observed trend demonstrated that the introduction of TES units into PBS chains resulted in a remarkable modification of the homopolymer mechanical properties and it can be ascribed to the different chemical composition and melting enthalpies (i.e. degree of crystallinity). The intrinsic characteristics of the three matrices and the interaction between each polymer and the different amount of added s-CNC, strongly affect the mechanical behavior of the studied nanocomposites. In particular, as to the stiff PBS homopolymer, the mechanical properties resulted slightly reduced, probably due to the presence of surfactant. On the contrary, the behavior of P(BS85TES15) copolymer was not affected by 1%wt of s-CNC, whereas 1%wt s-CNC already contributed to improve the elastic modulus and stress at break of P(BS70TES30). On the other hand, a higher content of cellulose nanocrystals (5%wt) significantly affected the mechanical response of the films, inducing an evident increase of the Young's modulus and a decrease of the elongation at break. The decrease of the elongation at break due to the presence of micro and nanostructures is a usual trend previously observed in thermoplastic and bio-based nanocomposites. The extent of this effect is influenced by various factors, such as the weight content of reinforcement, its dispersion in the matrix, and the interaction between the reinforcement and the polymer matrix (Fortunati, et al., 2012; Colom, Carrasco, Pages, & Canavate, 2003; Gupta, et al., 2009; Gupta, et al., 2010). In addition, s-CNC can cause substantial local stress concentrations in the polymer matrices.

The mechanical behavior of 5%wt s-CNC nanocomposites is influenced by two main factors: the different interaction between cellulose nanocrystals and the three polymeric matrices, and the high amount of the added nanoreinforcement. The higher stiffness of homopolymeric PBS matrix had indeed a synergic effect with the rigid cellulose nanocrystal, producing a general improvement of the mechanical properties as evident in PBS/5s-CNC system. On the contrary, the presence of TES units probably emphasized the effect of local stress concentration caused by high content of s-CNC, and had a more significant effect on the strain at break as compared to the other properties. Finally, a higher content of TES units could soften the stress localization, producing improved mechanical responses with respect to the neat P(BS70TES30) matrix.

The surfactant presence improves the dispersion of the s-CNC in the polymer matrix and also affects the ductile behavior of the films (Fortunati et al. 2012, Bondeson and Oksman, 2007). The interaction between cellulose nanocrystals and polymeric matrix is of great importance for the functional application of the new developed bio-based films. The mechanical properties results confirmed the reinforcement effect of the modified CNC and the role of the surfactant in the dispersion of CNC in the polymer matrices.

3.5. Optical properties

Figure 4 shows the values of gloss at 60º and internal transmittance (T_i) at 450 nm values of PBS and P(BSxTESy) based nanocomposites (a) and the optical microscopy images of the surface of PBS, and nanocomposite films (b).

The gloss and transparency of the films are important properties for final practical applications in some different industrial sectors (Muriel-Galet, et al., 2014).

The results of gloss analysis revealed that the presence TES co-units along the PBS backbone is able to influence the optical properties of the produced films. A relevant

increase of the gloss values was registered when 15% and 30% of TES sequences were introduced. Moreover, the gloss values of nanocomposite films reinforced with cellulose nanocrystals was greatly affected by both the presence and content of cellulosic nanoreinforcements, if compared with those registered for neat polymers (Figure 4a). A decrease of the gloss value was indeed observed as a function of filler percentage (Luzi, et al., 2016) and this effect was remarkably evident in the case of formulations loaded with the higher content (5%wt) of s-CNC that showed the lowest values of gloss at 60°. This result can be correlated to the presence of some small filler agglomerates shown on the surface of nanocomposite more evident when the highest content of cellulose nanocrystals (5%wt) was added, as observed in the optical microscopy images in the Figure 4b for PBS based systems. Similar results in terms of surface optical microscopy, were also obtained for P(BS85TES15) and P(BS70TES30) based formulations (data do not shown).

The internal transmittance (T_i) of different formulations was also evaluated and no particular differences were detected for P(BSxTESy) copolymers with respect to PBS (all values are around 80%). According to Kubelka-Munk theory, high values of T_i are associated to structural homogeneity and their degree of transparency, while low values are a consequence of a high structural heterogeneity and greater opacity (Jiménez, et al., 2012). The high values registered for PBS and P(BSxTESy) highlighted the homogeneity and transparency of the matrices used during the process that were poorly affected by the presence of cellulosic reinforcements. Lower values of T_i were instead registered for P(BS85TES15) based nanocomposites that showed a 72.2±1.2% and 69.5±0.7% for P(BS85TES15)/1s-CNC and P(BS85TES15)/5s-CNC, respectively. Heterogeneous structures are able to increase the light dispersion and at the same time to cause a reduction of internal transmittance (Cano, et al., 2015).

These results confirm the greater opacity and the reduction to UV radiation of film reinforced with cellulose nanocrystals previously observed by other authors (Arrieta, et al., 2014).

3.6.Wettability

To evaluate the relative hydrophilicity of the polymeric films under study, water contact angle (WCA) measurements have been performed. The contact angle values are reported in Table 2. As to the neat polymers, data showed that PBS is the more hydrophobic material, while the copolymer surface wettability is affected by the chemical composition: the higher the amount of TES co-units, the higher the wettability. This result is due to the presence along the polymeric chain of highly electronegative ether-oxygen atoms contained in the TES co-units (Figure 1), as already reported in the literature (Genovese et al. 2014; Gigli et al., 2014). The introduction of an increasing amount of s-CNC, influenced the surface wettability of each polymer, too. Indeed, by increasing the content of nanofiller, the wettability increased (Table 2), as a consequence of the presence of the cellulose hydroxyl groups (Moreno, et al., 2016).

The characterization techniques performed so far highlighted that P(BS70TES30) and its nanocomposites displayed the most promising characteristics, especially in terms of mechanical properties. In the light of the above reported results, these samples have therefore been chosen for further characterization.

3.7. Overall migration with food simulants

The results of the overall migration tests for P(BS70TES30), P(BS70TES30)/1s-CNC and P(BS70TES30)/5s-CNC formulations are shown in Figure 5. The idea was to demonstrate the possible practical application of the produced nanocomposite films as novel food packaging solutions.

After 2 days of incubation at 20 °C in isooctane, the maximum migration level was 0.11 mg kg^{-1} of simulant measured for all the studied formulations. It is worth noticing that the registered value is well below the migration limits for food contact materials (60 mg kg^{-1}), established by the European legislation (Commission Regulation EU 10/2011). Furthermore, no evident differences were induced by the presence of two percentages of s-CNC added to P(BS70TES30) formulations. Higher migration values were registered for all the studied formulations after 10 days of incubation at 40 °C in ethanol 10 % (v/v). The higher migration values induced by this simulant confirm the contact angle data, suggesting a more pronounced hydrophilicity of the system induced by the presence of 30% of TES co-units along the PBS main chain. However, all the migration values for the different formulations are below the legislative limits, confirming the possibility to employ the proposed materials as food-packaging.

3.8. Degradation in composting conditions

Composting studies have been carried out on P(BS70TES30), P(BS70TES30)/1s-CNC and P(BS70TES30)/5s-CNC, to evaluate the effect of the presence of the nanofiller on the biodegradation rate. The proceeding of the degradation has been monitored by weight loss measurements and the results obtained have been reported in Figure 6a. The three samples underwent a significant mass loss in the time scale explored. After 30 days of incubation P(BS70TES30)/1s-CNC and P(BS70TES30)/5s-CNC lost about 57% and 59% of their initial mass, respectively. On the other hand, the neat polymer degraded to a higher extent. Indeed, the mass loss at the end of the experiment reached 95%. This result is quite surprising, considering that both the degree of crystallinity and the surface wettability, two well-known parameters affecting the degradation rate of polymers (Gigli et al., 2013), would have supported opposite findings. Indeed, the three samples have a comparable crystallinity degree (Table 2) and the surface hydrophilicity increases with the increasing of the s-CNC

content (Table 2). As already reported in the literature for PLA-based nanocomposites containing CNC, the results can be explained as due to higher resistance to water uptake and diffusion through the nanocomposites with respect to the neat polymer induced by the CNC (Bitinis et al., 2013). Figure S6 displays the images of the partially degraded samples. An opacity increase already after 4 days of incubation and a significant fragmentation after 15 days can be observed, indicating the progress of the degradation.

Opacity increase can be due to different factors, such as formation of low molecular weight compounds, water uptake and higher crystallinity degree (Bitinis et al., 2013). It is important to point out that more accessible and less packed amorphous regions are preferentially attacked during the first stages of degradation. Moreover, the composting temperature, i.e. 58 °C, is comprised between the T_g and the T_m of the samples under study, thus annealing may occur. The above-mentioned phenomena gave rise to an increase of the degree of crystallinity during composting. To evaluate the evolution of the degree of crystallinity over the composting time, X-ray analyses have been performed and the results are reported in Table S1. Figure 6c contains the XRD patterns of the partially degraded films. In all cases, an increment of X_c with the increase of composting time can be observed, although some differences can be highlighted. The neat polymer displayed in fact a much higher variation of the degree of crystallinity as compared to the nanocomposites (Table S1). These findings are in good agreements with the weight losses.

The surface morphology of the partially degraded samples has been observed by SEM (Figure 6b). Before composting, the threes samples displayed a quite smooth surface. On the contrary, already after four days of incubation, large damaged areas with cracks and holes appeared on the film surface. The extent and entity of the degraded areas increased with the increase of the incubation time (Figure 5b).

4. Conclusions

The present work has been focused on the preparation of eco-friendly nanocomposites based on poly(butylene succinate) and containing ether-oxygen sequences in the polymer backbone and modified cellulose nanocrystals as fillers. The main outputs can be summarized as follows:

- the control over the reaction conditions allowed for the synthesis of high molecular weight copolymers with a random structure and a chemical composition close to the feed;
- the optimized extrusion process permitted the preparation of bionanocomposite films displaying a uniform dispersion of the CNC within the polymer matrix;
- by combining two different strategies, i.e. copolymerization and nanofiller addition, it has been possible to produce thin extruded films with a tunable range of properties by varying the amount and comonomeric unit (TES sequences) and/or of the nanofiller (s-CNC).

In particular it can be underlined that:

- with the increase of the TES co-unit mol%, the degree of crystallinity, the elastic modulus and the stress at break of the PBS homopolymer decreased, while the surface hydrophilicity increased;
- the presence of the s-CNC exerted a reinforcement effect on the polymer matrix, without compromising its original thermal properties;
- the migration tests and the optical property evaluations evidenced the suitability of the studied nanocomposites for packaging applications;
- the composting experiments evidenced a significant degradation rate after 30 days of incubation.

In conclusion, the combination of synthesized biodegradable polymers with bio-based nanostructures allowed for the development of advanced functional materials capable of meeting the requirements for a wide range of applications.

References

Arrieta et al., 2014 Arrieta, M., Fortunati E, Dominici F, Rayo´n E, Lopez J, Kenny JM (2014) LA-PHB/cellulose based films: mechanical, barrier and disintegration properties. *Carbohydrate Polymers, 107*, 139–149

Bitinis et al., 2013 Bitinis, N., Verdejo, R., Bras, J., Fortunati, E., Kenny, J.M., Torre, L., López-Manchado, M.A. (2013). Poly(lactic acid)/Natural rubber/Cellulose nanocrystal bionanocomposites Part II. Properties evaluation. *Carbohydrate Polymers, 96*, 621–627.

Bondeson and Oksman, 2007 Dispersion and characteristics of surfactant modified cellulose whiskers nanocomposites. (2007). *Composite Interfaces 14*, 617–630.

Braun et al., 2012 Braun, B., Dorgan, J.R., Hollingsworth, L.O. (2012) Supra-molecular ecobionanocomposites based on polylactide and cellulosic nanowhiskers: synthesis and properties. *Biomacromolecules, 13*, 2013–2019

Cano et al., 2015 Cano, A., Fortunati, E., Cha´fer, M., Gonza´lez-Martı´nez, C., Chiralt, A., Kenny, J.M. (2015). Effect of cellulose nanocrystals on the properties of pea starch–poly(vinyl alcohol) blend films. *Journal Material Science, 5*0, 6979–6992.

Colom, Carrasco, Pages, & Canavate, 2003 Colom, X., Carrasco, F., Pages, P., Canavate, J. (2003). Effects of different treatments on the interface of HDPE/lignocellulosic fiber composites. *Composite Science and Technology, 63*, 161–169.

Drufesne, 2013 Dufresne, A. (2013). Nanocellulose: A new ageless bionanomaterial. *Materials Today 16*, 220–227.

Fabbri et al., 2014 Fabbri, M., Gigli, M., Gamberini, R., Lotti, N., Gazzano, M., Rimini, B., Munari, A. (2014). Hydrolysable PBS-based poly(ester urethane)s thermoplastic elastomers. *Polymer Degradation& Stability, 108*, 223-231.

Fortunati et al., 2012 Fortunati, E., Armentano, I., Zhou, Q., Iannoni, A., Saino, E., Visai, L., Berglund, L.A., Kenny, J.M. (2012). Multifunctional bionanocomposite films of poly(lactic acid), cellulose nanocrystals and silver nanoparticles. *Carbohydrate Polymers, 87*, 1596–1605.

Fortunati et al., 2014 Fortunati, E., Rinaldi, S., Peltzer, M., Bloise, N., Visai, L., Armentano, I., Jiménez, A., Latterini, L., Kenny, J.M. (2014). Nano-biocomposite films with modified cellulose nanocrystals and synthesized silver nanoparticles. *Carbohydrate Polymers, 101*, 1122-1133.

Genovese et al., 2014 Genovese, L., Gigli, M., Lotti, N., Gazzano, M., Siracusa, V., Munari, A., Dalla Rosa, M. (2014). Biodegradable Long Chain Aliphatic Polyesters Containing Ether-Linkages: Synthesis, Solid-State, and Barrier Properties. *Industrial & Engineering Chemistry Research, 53*, 10965-10973.

Gigli et al., 2013 Gigli, M., Negroni, A., Soccio, M., Zanaroli, G., Lotti, N., Fava, F., Munari, A. (2013). Enzymatic hydrolysis studies on novel eco-friendly aliphatic thiocopolyesters, *Polymer Degradation & Stability, 98*, 934 - 942.

Gigli et al. 2014 Gigli, M., Lotti, N., Gazzano, M., Siracusa, V., Finelli, L., Munari, A., Dalla Rosa, M. (2014). Biodegradable aliphatic copolyesters containing PEG-like sequences for sustainable food packaging applications. *Polymer Degradation and Stability, 105*, 96-106.

Gigli, et al., 2016 Gigli, M., Fabbri, M., Lotti, N., Gamberini, R., Rimini, B., Munari, A. (2016). Poly(butylene succinate)-based polyesters for biomedical applications: a review. *Eur. Polym. J.*, 75, 431–460.

Gupta, et al., 2009 Gupta, M., Lin, Y.J., Deans, T., Crosby, A., Baer, E., Hiltner, A., Schiraldi, D.A. (2009). Biaxially oriented poly(propylene-g-maleic anhydride)/phosphate glass composite films for high gas barrier applications. *Polymer*, 50(2), 598-604.

Gupta, et al., 2010 Gupta, M., Lin, Y.J., Deans, T., Baer, E., Hiltner, A., Schiraldi, D.A. (2010). Structure and gas barrier properties of poly(propylene-g-maleic anhydride)/phosphate glass composites prepared by microlayer coextrusion. *Macromolecules*, 43(9), 4230-4239.

Habibi, Lucia, & Rojas 2010 Habibi, Y., Lucia, L.A., Rojas, O.J. (2010). Cellulose nanocrystals: chemistry, self-assembly, and applications. *Chemical Review, 110*, 3479–3500.

Heux, et al., 2000 Heux, L., Chauve, G., Bonini, C. (2000). Nonflocculating and chiral-nematic self-ordering of cellulose microcrystals suspensions in nonpolar solvents. *Langmuir*, 16, 82102.

Ichikawa et al., 2000 Ichikawa, Y., Kondo, H., Igarashi, Y., Noguchi, K., Okuyama, K., Washiyama, J. (2000). Crystal structures of a and b forms of poly(tetramethylene succinate). *Polymer 41*, 4719–4727. corrigendum, *Polymer, 42*, 847–847.

Jiménez et al., 2012 Jiménez, A., Fabra, M.J., Talens, P., Chiralt, A. (2012). Effect of re-crystallization on tensile, optical and water vapour barrier properties of corn starch films containing fatty acids. *Food Hydrocolloids*, *26*, 302–310.

Khalil et al., 2014 Khalil, F., Galland, S., Cottaz, A., Joly, C., Degraeve, P. (2014). Polybutylene succinate adipate/starch blends: A morphological study for the design of controlled release films, Fadi Khalil, Sophie Galland, Amandine Cottaz, Catherine Joly,P ascal Degraeve, *Carbohydrate Polymers 108*, 272–280.

Kim et al. 2006 Kim, H.S, Kim, H.J., Lee, J.W., Choi, I.G. (2006). Biodegradability of bio-flour filled biodegradable poly(butylene succinate) bio-composites in natural and compost soil. *Polymer Degradation &Stability 91*, 1117-1127;

Klemm et al., 2005 Klemm, D., Heublein, B., Fink, H.-P., Bohn, A. (2005). Cellulose: fascinating biopolymer and sustainable raw material. *Angew Chem Int Ed 44*, 3358–3393.

Lizundia et al.: 2016 Lizundia, E., Fortunati, E., Dominici, F., Vilas, J.L., León, L.M., Armentano, I., Torre , L., Kenny, J.M. (2016). PLLA-grafted cellulose nanocrystals: Role of the CNC content and grafting on the PLA bionanocomposite film properties. *Carbohydrate Polymers 142*, 105–113.

Luzi et al., 2016 Luzi, F., Fortunati, E., Jiménez, A., Puglia, D., Pezzolla, D., Gigliotti, G., Kenny, J.M., Chiralt, A., Torre, L. (2016). Production and characterization of PLA_PBS biodegradable blends reinforced with cellulose nanocrystals extracted from hemp fibres *Industrial Crops and Products* DOI:10.1016/j.indcrop.2016.01.045, in press.

Moon et al., 2011 Moon, R.J., Martini, A., Nairn, J., Simonsen, J., Youngblood, J. (2011). Cellulose nanomaterials review: structure, properties and nanocomposites. *Chem Soc Rev 40*, 3941–3994.

Moreno et al., 2016 Moreno, M., Armentano, I., Fortunati, E., Mattioli, S., Torre, L, Lligadas, G., Ronda, J.C., Galià, M. Cádiz, V. (2016). Cellulose nano-biocomposites

from high oleic sunflower oilderived thermosets. *European Polymer Journal 79* 109–120.

Muriel-Galet et al., 2014 Muriel-Galet, V., López-Carballo, G., Hernández-Muñoz, P., Gavara, R. (2014). Characterization of ethylene-vinyl alcohol copolymer containing laurel arginate (LAE) as material for active antimicrobial food packaging. *Food Packaging and Shelf Life 1*, 10–18.

Soccio et al., 2012 Soccio, M., Lotti, N.,Gigli, M., Finelli, L., Gazzano, M., Munari, A. (2012). Reactive blending of poly(butylene succinate) and poly(triethylene succinate): characterization of the copolymers obtained. *Polym Int 61*, 1163–1169.

Song et al., 2014 Song, Z., Xiao, H., & Zhao, Y. (2014). Hydrophobic-modified nano-cellulose fiber/PLA biodegradable composites for lowering water vapor transmission rate (WVTR) of paper. *Carbohydrate Polymers*, *111*, 442–448

Zakharova et al., 2015 Zakharova, E., Alla, A., Martinez de Ilarduya, A., Muñoz-Guerra, S. (2015). Bio-based PBS copolyesters derived from a bicyclic D-glucitol, *RSC Adv. 5*, 46395–46404

Zhang&Zhang, 2016 Reinforcement effect of poly(butylene succinate) (PBS)-grafted cellulose nanocrystal on toughened PBS/polylactic acid blends. *Carbohydrate Polymers 140*, 374–382.

Figure and Table Caption

Figure 1. Chemical structure and 1H-NMR of the synthetized polyesters. In the insets the expansion of the **a** methylene of the succinic subunit region between 2.75 and 2.55 ppm.

Figure 2. FESEM fractures of polymer and nanocomposite films

Figure 3. Calorimetric curves of PBS-based nanocomposites. a) I scan, b) II scan after quenching, c) crystallization from the melt.

Figure 4. a) Gloss at 60º and internal transmittance (T_i) at 450 nm values of PBS and P(BSxTESy) based nanocomposites; b) optical microscopy images of the surface of PBS, and nanocomposite films.

Figure 5. Overall migration in 10% (v/v) ethanol and isooctane for PBS and P(BSTES) based nanocomposites.

Figure 6. Degradation in compost. A) gravimetric weight loss, b) SEM micrographs, C) evolution of the XRD patterns as a function of the incubation time

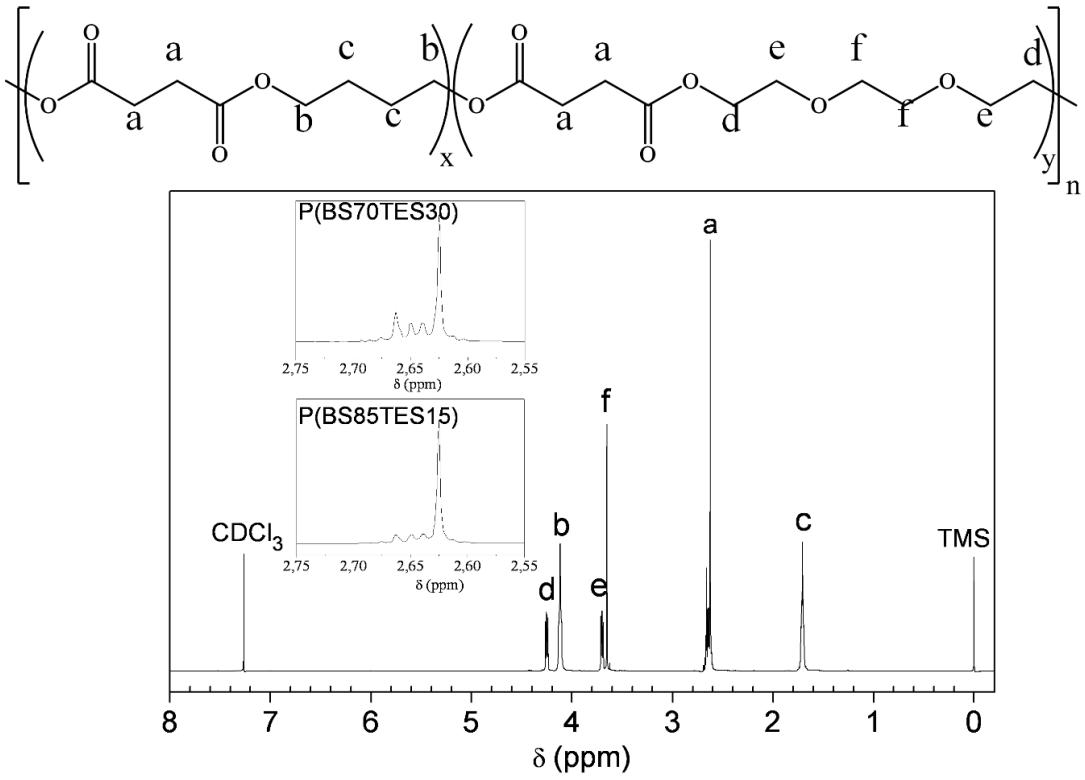

Figure 1. Chemical structure and 1H-NMR of the synthetized polyesters. In the insets the expansion of the **a** methylene of the succinic subunit region between 2.75 and 2.55 ppm.

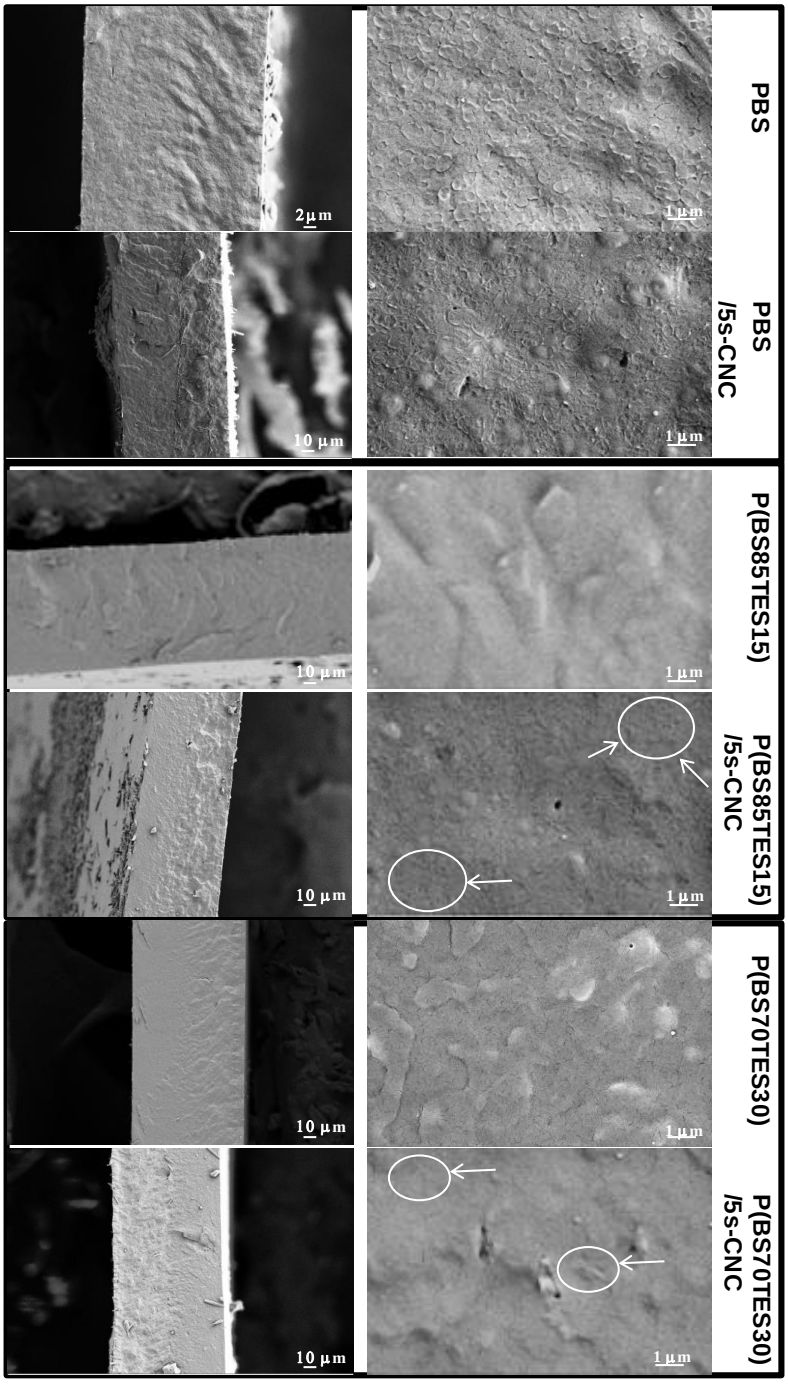

Figure 2. FESEM fractures of polymer and nanocomposite films

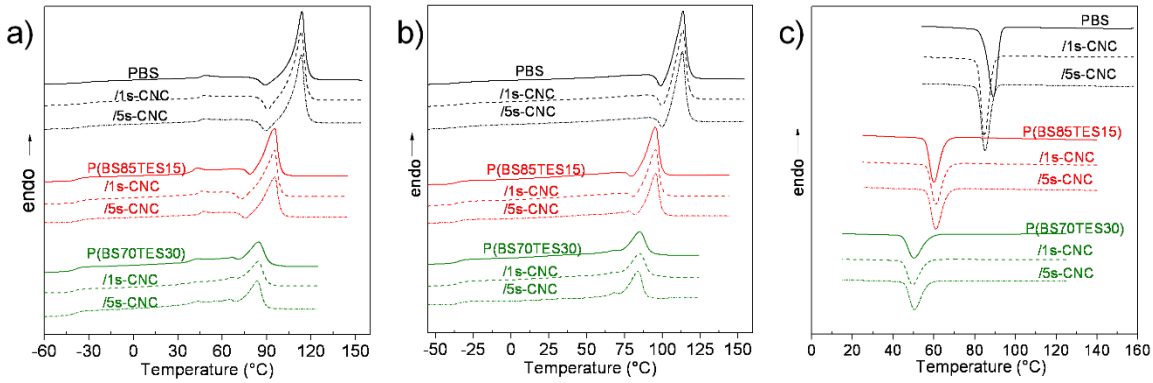

Figure 3. Calorimetric curves of PBS-based nanocomposites. a) I scan, b) II scan after quenching, c) crystallization from the melt.

a)

Formulations	*Gloss Values (°)*	*Internal transmittance (%)*
	Gloss at 60 °	*Ti (450 nm)*
PBS	32±3	80±1
PBS/1s-CNC	19±1	78±1
PBS/5s-CNC	13±2	75±1
P(BS85TES15)	57±1	80±1
P(BS85TES15)/1s-CNC	45±3	72±1
P(BS85TES15)/5s-CNC	26±2	70±1
P(BS70TES30)	63±3	80±1
P(BS70TES30)/1s-CNC	50±2	77±1
P(BS70TES30)/5s-CNC	32±1	77±1

b)

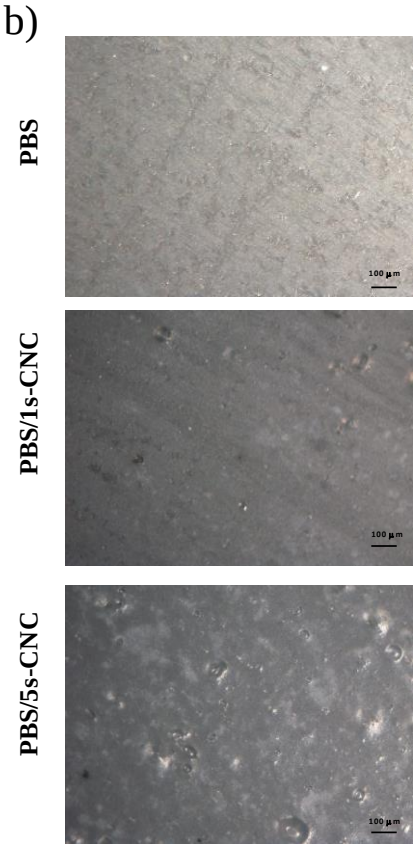

Figure 4: a) Gloss at 60º and internal transmittance (T_i) at 450 nm values of PBS and P(BSxTESy) based nanocomposites; b) optical microscopy images of the surface of PBS, and nanocomposite films.

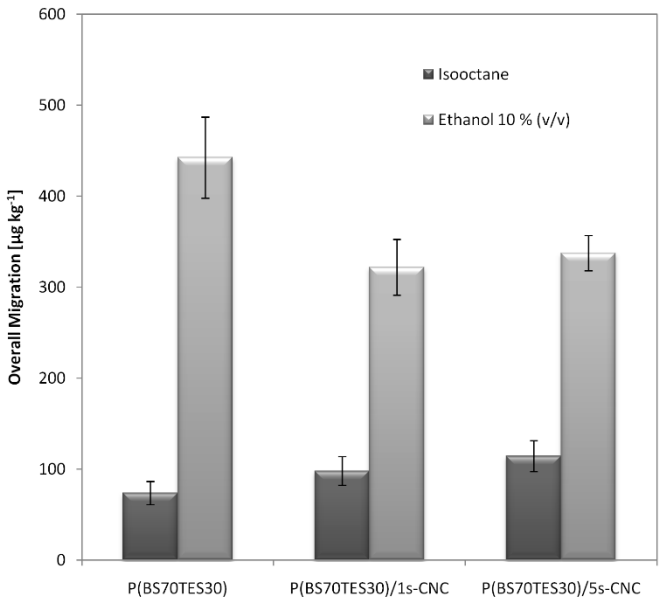

Figure 5. Overall migration in 10% (v/v) ethanol and isooctane for PBS and P(BSTES) based nanocomposites.

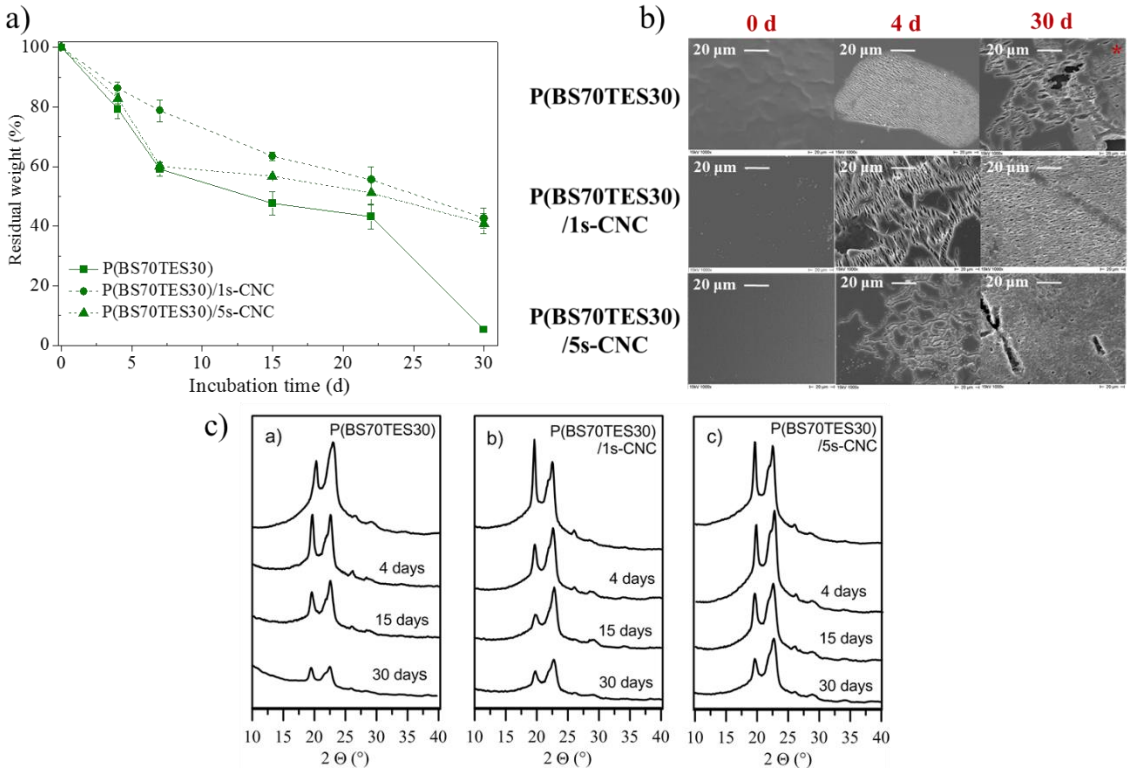

Figure 6. Degradation in compost. A) gravimetric weight loss, b) SEM micrographs, C) evolution of the XRD patterns as a function of the incubation time

Table 1: Molecular characterization data, material formulations and process parameters.

Formulations	***Polymer molecular properties***				***Component Content***		***Temperature Profiles (°C)***
	TES[a] (mol%)	***b[b]***	***M_n[c]***	***PDI[c]***	***Polymer (%wt)***	***s-CNC (%wt)***	
PBS	/	/	50600	3.0	100	-	130-135-145
PBS/1s-CNC					99	1	130-135-145
PBS/5s-CNC					95	5	130-135-145
P(BS85TES15)	16.9	1.03	38100	3.1	100	-	120-125-135
P(BS85TES15)/1s-CNC					99	1	120-125-135
P(BS85TES15)/5s-CNC					95	5	120-125-135
P(BS70TES30)	33.8	1.02	39000	3.3	100	-	105-110-120
P(BS70TES30)/1s-CNC					99	1	105-110-120
P(BS70TES30)/5s-CNC					95	5	105-110-120

[a] determined by 1H-NMR
[b] degree of randomness, determined by 1H-NMR
[c] M_n: number average molar mass and PDI: polydispersity index, determined by gel permeation chromatography (GPC)

Table 2: Thermal, wettability and mechanical properties of polymer and nanocomposite films.

	I scan			*II scan*								
Formulations	T_g *(°C)*	T_m *(°C)*	ΔH_m *(J/g)*	T_g *(°C)*	T_m *(°C)*	ΔH_m *(J/g)*	T_c *(°C)*	T_{max} *(°C)*	*WCA (°)*	σ_B *(MPa)*	ε_B *(%)*	*E (MPa)*
PBS	-34±1	114±1	60±3	-34±1	114±1	58±4	89±1	402±1	82 ± 1	40±2	220±60	430±50
PBS/1s-CNC	-33±1	113±1	65±4	-33±1	114±1	62±2	85±1	402±1	79 ± 1	34±8	180±70	372±25
PBS/5s-CNC	-33±1	113±1	65±3	-34±1	113±1	63±2	85±1	402±1	73 ± 1	50±3	220±60	558±20
P(BS85TES15)	-36±1	95±1	51±4	-38±1	95±1	47±3	60±1	407±1	73 ± 2	34±4	252±24	391±20
P(BS85TES15) /1s-CNC	-36±1	95±1	48±5	-37±1	96±1	45±3	61±1	407±1	71 ± 1	33±5	230±60	350±50
P(BS85TES15) /5s-CNC	-36±1	96±1	49±3	-37±1	96±1	46±2	61±1	407±1	67 ± 3	27±3	160±50	332±24
P(BS70TES30)	-37±1	85±1	30±2	-39±1	85±1	29±2	50±1	404±1	66 ± 2	19±2	350±70	162±27
P(BS70TES30) /1s-CNC	-37±1	84±1	29±1	-40±1	85±1	27±2	50±1	404±1	64 ± 3	26±3	270±60	239±29
P(BS70TES30) /5s-CNC	-37±1	84±1	32±3	-40±1	84±1	31±1	50±1	404±1	56 ± 4	22±2	240±50	233±28

T_g: glass transition temperature, T_m: melting temperature, ΔH_m: enthalpy of fusion, T_c: crystallization temperature, determined by DSC
T_{max}: temperature of the maximum degradation rate, determined by TGA
WCA: water contact angle
σ_B *:* tensile strength, ε_B *:* elongation at break, E: Young's modulus determined by tensile testing